

Adsorption of maleic acid monomer on the surface of hydroxyapatite and TiO_2 : a pathway toward biomaterial composites

Mitchell Albert, Amanda Clifford, Igor Zhitomirsky,* and Oleg Rubel*

Department of Materials Science and Engineering, McMaster University, 1280 Main Street West, Hamilton, Ontario L8S 4L8, Canada

E-mail: zhitom@mcmaster.ca; rubelo@mcmaster.ca

Phone: +1 905 5259140 ext. 24295

Abstract

Poly(styrene-alt-maleic acid) adsorption on hydroxyapatite and TiO_2 (rutile) was studied using experimental techniques and complemented by *ab initio* simulations of adsorption of a maleic acid segment as a subunit of the copolymer. *Ab initio* calculations suggest that the maleic acid segment forms a strong covalent bonding to the TiO_2 and hydroxyapatite surfaces. If compared to vacuum, the presence of a solvent significantly reduces the adsorption strength as the polarity of the solvent increases. The results of first-principle calculations are confirmed by the experimental measurements. We found that adsorbed poly(styrene-alt-maleic acid) allowed efficient dispersion of rutile and formation of films by the electrophoretic deposition. Moreover, rutile can be co-dispersed and co-deposited with hydroxyapatite to form composite films. The coatings showed an enhanced corrosion protection of metallic implants in simulated body fluid solutions, which opens new avenues for the synthesis, dispersion, and colloidal processing of advanced composite materials for biomedical applications.

Keywords

Maleic acid monomer, hydroxyapatite, rutile, surface adsorption, density functional theory, electrophoretic deposition, coating, corrosion protection

1 Introduction

Investigations of adsorption of organic molecules at the surface of nanomaterials and their colloidal behaviour¹ allowed for the development of novel strategies for the surface modification, dispersion, and advanced synthesis of nanoparticles. Studies of mussel adsorption on inorganic surfaces^{2,3} provide important chemical and physical insights into development of covalent anchoring mechanisms. It was found that the strong mussel adhesion involves protein macromolecules that contain a catecholic amino acid L-3,4-dihydroxyphenylalanine (L-DOPA). The adhesion mechanism of mussels is attributed to the complexation, or bridging bidentate bonding between metal atoms on material surfaces and hydroxyl groups of catechol.⁴ These studies have generated interest in the investigation of catecholates and inspired the development of advanced adhesives,^{3,5} dispersants,⁶ liquid-liquid extraction agents⁷⁻¹⁰ containing anchoring catechol groups for various applications (see Ref. 11 and references therein).

The success in the applications of chelating molecules from the catechol family has driven investigations of natural aliphatic compounds with carboxyl groups, which can provide strong chelating or bridging polydentate bonding to inorganic materials. Of particular interest are fumaric and maleic acid (MA) isomers, containing *trans* and *cis* carboxyl groups, respectively. These acids showed strong adsorption on various oxides.¹² The *cis* conformation of maleic acid provides an ideal orientation for coordination *via* both carboxylate groups in a strong tetradentate interaction.^{12,13} It is in this regard that many dispersant molecules described in the literature provide a relatively weak monodentate bonding to the particle surface.^{6,14-17} Clearly, tetradentate interactions of maleic acid with oxide surfaces offer ad-

vantages for surface modification of materials.

Significantly stronger interactions with inorganic surfaces can be expected using maleic acid polymers or copolymers. The individual maleic acid monomers of such polymers can provide multiple chemical bonds with substrates. Poly(maleic acid) showed a strong adsorption on alumina particles and allowed for their efficient dispersion.¹⁸ Poly(acrylic acid-co-maleic acid) exhibited a strong affinity to BaTiO₃ and clay minerals.^{19,20} The adsorption properties of poly(styrene-alt-maleic acid) (PSMA-h) copolymer (Fig. 1) have been utilized for the synthesis of inorganic particles with different morphologies^{21–23} and unusual superstructures.²⁴ PSMA-h is a biocompatible polymer, which is currently under investigations for many biomedical applications, such as drug delivery,^{25–27} biosensors,²⁸ antimicrobial materials²⁹ and implants.^{30,31} PSMA-h demonstrated a strong affinity to hydroxyapatite (HA), bio-glass, and bioceramics and allowed their electrophoretic deposition (EPD) and co-deposition with proteins.³² Colloidal techniques, such as EPD, have a high potential in the development of advanced films, coatings, scaffolds and devices for biomedical applications. Therefore, the investigation of PSMA-h adsorption on bioceramics opens new avenues for the synthesis, dispersion, and colloidal processing of advanced materials for biomedical applications.

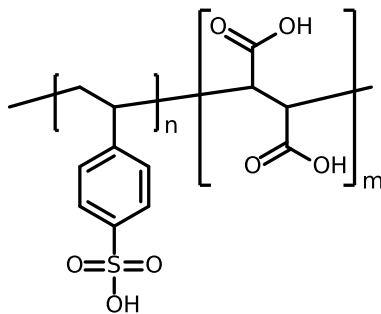


Figure 1: Styrene-maleic acid copolymer.

HA is an important material for biomedical implant applications, because its chemical composition is similar to that of natural bone.³³ Rutile is also known as a bioactive material, which promotes HA biomineralization.^{34–36} Compared to the anatase phase, the rutile phase of TiO₂ has many advantages for implant applications, such as phase stability, chem-

ical stability and improved corrosion protection.³⁷ The addition of rutile to the HA to form a composite coating offers many benefits, such as enhanced chemical stability, improved corrosion protection of implants, bioactivity, improved mechanical properties, enhanced osteoblast adhesion and cell growth.^{38–42} Previous investigations³² showed that HA coatings can be deposited by EPD using PSMA-h as a charging and dispersing agent, which strongly adsorbed on the HA surface.

The goal of this investigation was to probe the PSMA-h adsorption on HA and TiO₂ (rutile) using experimental techniques as well as to perform *ab initio* simulations of adsorption of a maleic acid segment as a subunit of the copolymer. We identified the most stable TiO₂ and HA surfaces and their reconstructions in the presence of a solvent using first-principle atomistic modelling. We examined molecular mechanisms and adsorption strength of MA on different surfaces of TiO₂ and HA. Our simulations indicate that two carboxylate functional groups of MA form strong covalent bonds at the surfaces of HA and TiO₂. In these calculations MA was treated as a segment of a polymer chain rather than a monomer. Our studies demonstrate that a solvent significantly alters the surface energy and adsorption characteristics of molecules. Experimental measurements are performed to test validity of the theory. The measurements include the use of PSMA-h as a dispersion agent for rutile and formation of films by EPD. We examined the deposition yield, film morphology, and corrosion resistance. The possibility of co-dispersing and co-depositing the rutile with HA to form composite films is investigated for biomedical applications.

2 Methods

2.1 Computational

The first-principle electronic structure calculations have been performed in the framework of the density functional theory (DFT)⁴³ using Perdew-Burke-Ernzerhof generalized gradient approximation (GGA-PBE) for the exchange-correlation functional.⁴⁴ The Vienna *ab initio*

simulation program (VASP) and projector augmented-wave potentials⁴⁵⁻⁴⁷ were used. Full self-consistent structural optimization was performed for the bulk TiO₂ (rutile) and HA. The structure was considered optimized when the magnitude of Hellmann-Feynman forces acting on atoms dropped below 10 meV/Å and components of the stress tensor did not exceed 1 kBar. The Brillouin zone was sampled using 3 × 3 × 4 and 2 × 2 × 4 Monkhorst-Pack grid⁴⁸ for TiO₂ and HA primitive cells, respectively. The cutoff energy for a plane wave expansion was set at 500 eV, which is 25% higher than the value recommended in the pseudopotential file for oxygen. The higher cutoff energy was essential for obtaining accurate structural parameters, which are summarized in Table 1. The theoretical lattice parameters are within 2% error of the experimental values that is typical for GGA-PBE. An attempt was made to include the on-site Coulomb interaction for Ti *d*-electrons in the framework of Dudarev et al.⁴⁹ using the effective Hubbard energy of $U = 2$ eV.⁵⁰ However, this correction resulted in a greater deviation between theoretical and experimental lattice parameters and thus was abandoned.

Table 1: Bulk structure properties (lattice parameters and fractional coordinates of atoms) of TiO₂ and HA. Theoretical results are obtained using DFT. The neutron diffraction experimental data for TiO₂ and HA are taken from Refs.^{51,52}

Compound	Calculated			Experiment		
	$a = b$ (Å)	c (Å)	u	$a = b$ (Å)	c (Å)	u
TiO ₂ (rutile)	4.664	2.966	O (0.3046, 0.3046, 0)	4.594	2.959	O (0.3048, 0.3048, 0)
Hydroxyapatite	9.549	6.934	Ca _I (1/3, 2/3, 0.0016)	9.432	6.881	Ca _I (1/3, 2/3, 0.0014)
			Ca _{II} (0.2501, 0.9986, 0.2513)			Ca _{II} (0.2466, 0.9931, 1/4)
			P (0.3988, 0.3682, 0.2524)			P (0.3982, 0.3682, 1/4)
			O _I (0.3301, 0.4850, 0.2538)			O _I (0.3283, 0.4846, 1/4)
			O _{II} (0.5877, 0.4638, 0.2470)			O _{II} (0.5876, 0.4652, 1/4)
			O _{III} (0.3379, 0.2549, 0.0737)			O _{III} (0.3433, 0.2579, 0.0705)

TiO₂ (110), HA (0001) and (01 $\bar{1}$ 0) surfaces are obtained on the basis of the optimized bulk structures. The 20 Å spacing between periodical images of slabs in direction perpendicular to the surface ensures no spurious interactions. The TiO₂ (110) slab is represented by four monolayers of Ti-atoms with a well-established surface termination that consists of alternating rows of 5- and 6-fold-coordinated Ti sites running along the [001] direction.^{53,54} The HA (0001) and (01 $\bar{1}$ 0) slabs are constructed using 9 and 7 monolayers of Ca-atoms, re-

spectively. There are some ambiguities about HA $(01\bar{1}0)$ surface and its reconstruction.^{55–57} Several scenarios for a stoichiometric cleavage surface were explored. The lowest surface energy corresponds to the cleavage plane selected such that PO_4 tetrahedra remain preserved (Fig. 2). It is this surface reconstruction that is later used for studying the adsorption of molecules. Atoms of the slab representing the surface were allowed to relax except for three monolayers in the centre of the slab that were constrained to the bulk atomic positions. The presence of a solid-liquid interface is modelled using an implicit solvation model implemented in VASPsol⁵⁸ and values of the static dielectric constant for a water-ethanol mixture tabulated in Ref. 59.

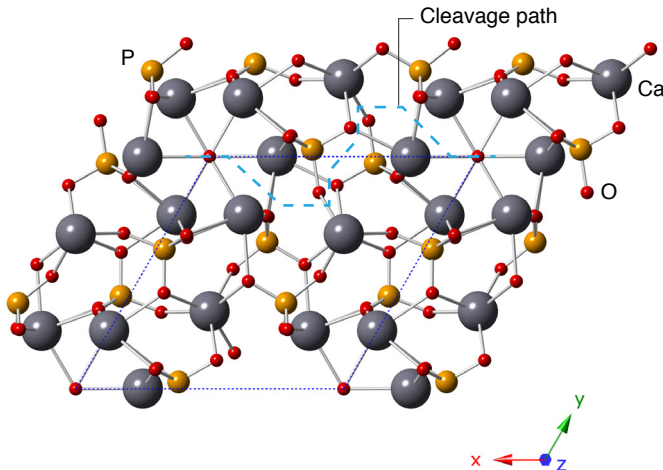


Figure 2: HA low-energy $(01\bar{1}0)$ stoichiometric surface is created by cleaving the slab along the dashed line. The construction maintains the integrity of PO_4 tetrahedra.

The MA molecular structure (Fig. 3a,b) is obtained by relaxing all degrees of freedom in a simulation box of the size $15 \times 15 \times 15 \text{ \AA}^3$ to prevent spurious interactions between periodical images. However, this molecule is not chemically equivalent to the MA being a segment of the copolymer. To model the MA segment, two hydrogen-terminated carbon atoms were added to the MA molecule such that they mimic a polymer chain (Fig. 3e,f). As a result, the sp^2 double bond between two carbon atoms in MA transforms into an sp^3 single bond in the MA segment. It is assumed that the individual MA segment can represent an MA residue as a part of copolymer and can serve as a basis for studying its adsorption at

inorganic surfaces. This choice is driven by the necessity to make our model computationally feasible at the first-principle level. At the same time, we admit that this approach omits some details of the copolymer confirmation that can limit exposure of MA residues to the solvent/surface and possible interactions between phenyl group and the surfaces.

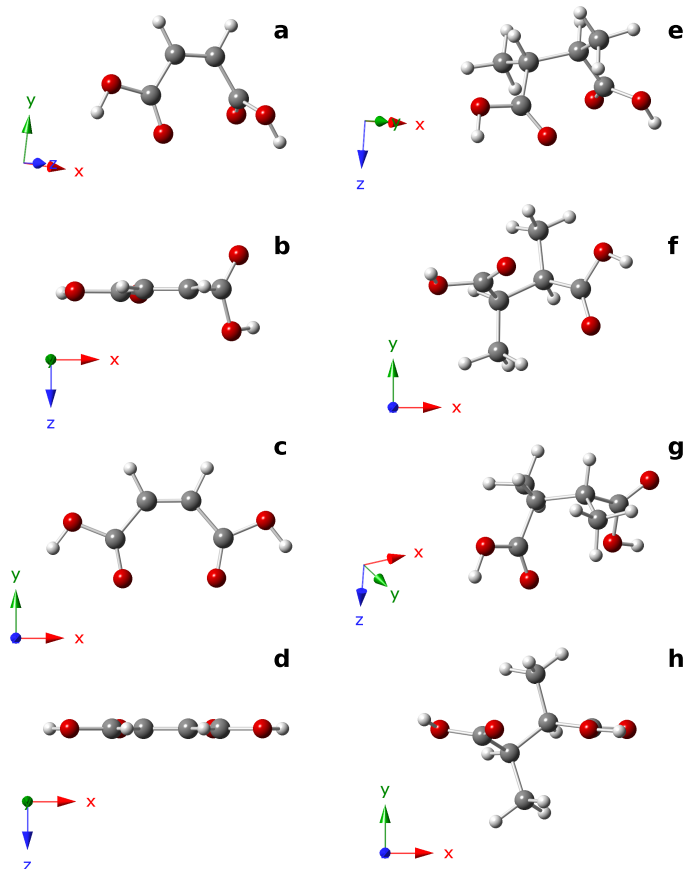


Figure 3: The structure of maleic acid as a monomer (a,b) 3D conformer, (c,d) 2D flattened conformer, and as a part of the polymer chain (e,f) 3D conformer, (g,h) 2D flattened carboxyl groups. The deformation energy associated with changing the confirmation 3D→2D is approximately 0.15 eV.

The adsorption of MA monomer and MA segment is modelled as an inner-sphere surface complex. The molecules were initially positioned at the surface in such a way that the distance and arrangement between the metal ion and oxygen atoms of the ligands resembles that in the bulk. The structural optimization is performed until Hellmann-Feynman forces acting on atoms dropped below 20 meV/Å. Crystallographic information files (CIF) with atomic structures used in calculations can be accessed through the Cambridge crystallographic data

centre (CCDC deposition numbers 1582972–1582992).

2.2 Experimental

Titanium foil (0.127 mm), TiO_2 (rutile, the particle size less than 100 nm), poly(styrene-alt-maleic acid), $\text{Ca}(\text{NO}_3)_2 \cdot 4\text{H}_2\text{O}$, $(\text{NH}_4)_2\text{HPO}_4$, NH_4OH , and Hank’s balanced salt solution (CaCl_2 0.14 g/L, KCl 0.40 g/L, KH_2PO_4 0.06 g/L, $\text{MgCl}_2 \cdot 6\text{H}_2\text{O}$ 0.10 g/L, $\text{MgSO}_4 \cdot 7\text{H}_2\text{O}$ 0.10 g/L, NaCl 8.00 g/L, NaHCO_3 0.35 g/L, Na_2HPO_4 0.048 g/L, glucose 1.00 g/L, phenol red 0.01 g/L, Sigma-Aldrich, Canada) were used for the following experiments. Stoichiometric HA was synthesized using wet chemical precipitation, by the slow addition of 0.6 M $(\text{NH}_4)_2\text{HPO}_4$ solution to 1.0 M $\text{Ca}(\text{NO}_3)_2$ solution while continuously stirring at 70°C . The solution was stirred for 8 h at 70°C , followed by 24 h of stirring at room temperature, and the pH was adjusted to 11 using NH_4OH . The resulting precipitate was washed using water and ethanol, then dried. Crystalline needle-shaped HA nanoparticles have been obtained using this method. A TEM micrograph presented in Fig. 4 shows a needle-shaped HA particle morphology. HA particles had an aspect ratio of approximately eight, and an average length of 150 nm.

Stainless steel or titanium foil were used as substrates for EPD. The substrate was placed 15 mm away from the platinum counter electrode. The deposition time was varied in the range of 1–6 mins, and deposition voltage was within the range of 10–15 V. TiO_2 and HA were dispersed in a mixed water-ethanol solvent (40% water), containing dissolved PSMA-h. The use of the mixed solvent offered the advantages of reduced gas evolution at the substrate surface. The deposition yield was studied using stainless steel substrates. Potentiodynamic studies were performed using a Parstat 2273 potentiostat and the PowerSuite software (Princeton Applied Research). A three-cell electrode cell was used for electrochemical testing, with a saturated calomel electrode (SCE) as the reference electrode and platinum mesh as the counter electrode. The test was carried out in Hank’s balanced salt solution, which was used to simulate physiological conditions. A scan rate of 1 mV/s was used to

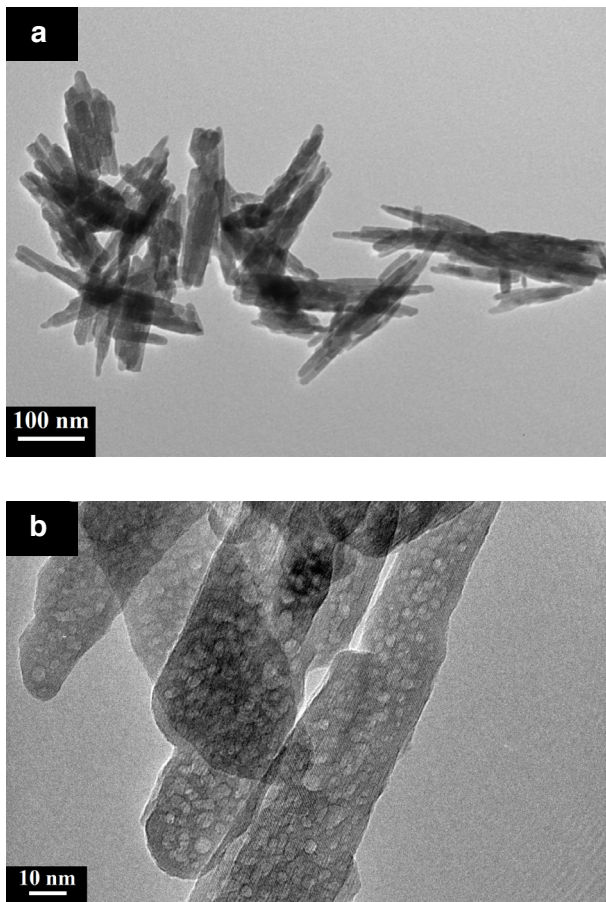


Figure 4: TEM images of hydroxyapatite particles at two different magnifications: (a) $\times 150,000$ and (b) $\times 10^6$.

obtain the potentiodynamic polarization curves.

A JEOL 7000F scanning electron microscope (SEM) and FEI Tecnai Osiris transmission electron microscope (TEM) were used for electron microscopy. A Nicolet I2 diffractometer with monochromatized CuK_α radiation was used for X-Ray diffraction (XRD). Fourier-transform infrared spectroscopy (FTIR) studies were performed on Bruker Vertex 70 spectrometer.

3 Results and discussion

We begin with examining surfaces of rutile and HA. The specific surface energy is defined as

$$\gamma = \frac{E_{\text{tot}}(\text{slab}) - E_{\text{tot}}(\text{bulk})}{2A}, \tag{1}$$

where E_{tot} is the DFT total energy of the slab and the bulk material, A is the planar surface area, and the factor of 2 accounts for the presence of two surfaces at the top and bottom of the simulation slab. Results for the surface energy are presented in Table 2, which also includes values of the surface energies reported in the literature for comparison. A large scattering of literature values, in particular for HA, can be attributed to variability in DFT approximations for the exchange-correlation functional, selection of pseudopotentials, and uncertainties in the structure specifically for the HA(01 $\bar{1}$ 0) surface. HA has a higher surface energy that correlates with its higher wettability in comparison to TiO_2 . The presence of a polar solvent (water) significantly affects the surface energy, in particular for HA. The disparity between the surface energies of TiO_2 and HA vanishes in the solvent.

MA molecule and MA segment adapt a three-dimensional structure as shown in Figs. 3a,b and 3e,f, respectively. Some adsorption configurations require a structural deformation (flattening) of the MA molecule or MA segment. The flattening occurs *via* rotating the carboxyl groups to align both groups to a common plane as illustrated in Figs. 3c,d and 3g,h, respectively. The associated deformation energy is of the order of 0.15 eV as evaluated by DFT

Table 2: Calculated surface energy and absorption energy of MA at TiO₂ and HA surfaces. Values are presented for various solvent conditions: vacuum/mixture 80% ethanol + 20% water/100% water, respectively.

Surface	Surface energy (J/m ²)	Adsorption enthalpy (eV)	
		monomer	segment
TiO ₂ (110)	0.63 ^a /0.48/0.44	-1.3/-0.7/-0.6	-1.3/-0.9/-0.6
HA (0001)	0.90 ^b /0.53/0.45	-3.4/-1.3/-1.2	—
HA (01 $\bar{1}$ 0)	0.96 ^c /0.59/0.51	-4.7/-2.5/-2.1	-4.0/-1.8/-1.5

^a 0.31–0.47, 0.89 J/m² (DFT calculations^{53,60}); ^b 0.33, 0.77, 1.01, 1.93 J/m² (DFT calculations^{55–57,61}); ^c 0.33, 1.32, 1.36, 2.10 J/m² (DFT calculations^{55–57,61})

calculations, which is one order of magnitude less than typical adsorption energies. The ability of MA to easily adapt its structure to the surface of interest can be attributed to its aliphatic nature.

Figure 5 shows the lowest energy configuration of MA monomer adsorbed on TiO₂ and HA surfaces. Adsorption to the TiO₂ surface takes place *via* an inner sphere bonding to a pair of Ti-atoms (a bridge bidentate coordination) as illustrated in Fig. 6a, rather than chelate bidentate bonding to a single Ti site at the surface. This result can be explained by a dense packing of Ti atoms at TiO₂ surface and is reminiscent of catecholates’ adsorption on TiO₂.^{11,62} In the case of HA, the spacing between Ca-atoms at the surface is too large. Therefore, chelation is a preferable type of bonding on HA (Fig. 6b,c). The adsorption of MA is accompanied by deprotonation of both carboxyl groups. Those protons are readily attracted to passivate oxygen dangling bonds at the surface PO₄-tetrahedra and to restore the charge balance perturbed by the newly formed Ti–O or Ca–O bonds.⁶² Regarding H⁺ placement on the HA(01 $\bar{1}$ 0) surface, there are several alternatives to the top of PO₄-tetrahedra, which include O-atoms in the base of PO₄-tetrahedra as well as the ≡Ca₂OH^{q-} groups present at the surface. It turns out that ≡Ca₂OH₂^{1-q} is the second most favourable scenario from DFT the total energy point of view.

The affinity of MA to the surfaces is characterized by the adsorption enthalpy, which is defined as

$$\Delta H_{\text{ads}} \approx E_{\text{tot}}(\text{MA ads.}) - E_{\text{tot}}(\text{MA}) - E_{\text{tot}}(\text{slab}), \quad (2)$$

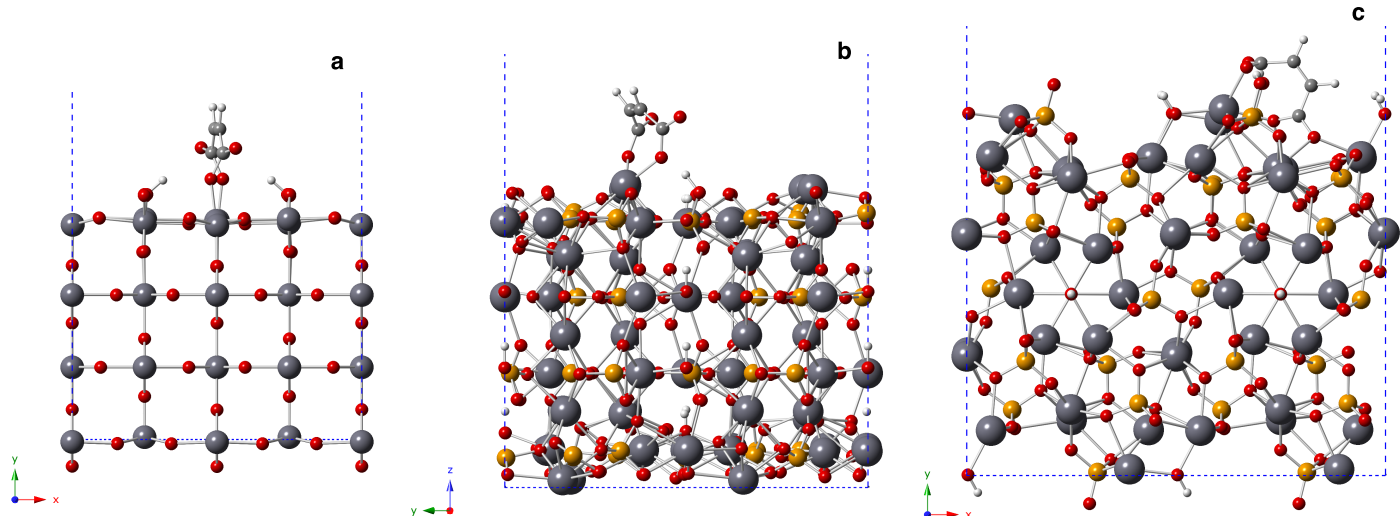


Figure 5: (a) Maleic acid monomer at the (110) surface of TiO_2 , (b) at the HA (0001) surface and (c) at the HA (0110) surface.

where $E_{\text{tot}}(\text{MA ads.})$ is the total energy of a slab with the molecule adsorbed on its surface (Fig. 5), $E_{\text{tot}}(\text{MA})$ is the total energy of the molecule or segment in its ground state configuration (Figs. 3a or 3e), and $E_{\text{tot}}(\text{slab})$ is the energy of the slab. The approximate sign reflects neglecting a zero-point energy change upon adsorption and finite temperature effects. This approximation is justified in an earlier study of catalytic reactions,⁶³ since the sum of zero-point energies is approximately constant during the traversing of regions with energy barriers.

The adsorption enthalpies of MA on TiO_2 and HA surfaces are summarized in Table 2. Here we list results obtained for different solvents: water, a mixture of water and ethanol as well as for the vacuum since effects of the solvent are often neglected in studies of a molecular adsorption. Values of the adsorption enthalpy in Table 2 suggest that the binding energies of molecules to the surface are significantly overestimated in vacuum (almost by a factor of two). The more ionic the solvent, the weaker is the affinity of MA to the surface. The adsorption enthalpies of MA on TiO_2 and HA surfaces in water remain strong: $\Delta H_{\text{ads}} = -0.6$ and -1.5 eV respectively, in spite of solvation effect. The values are comparable to -1 eV bond strength between DOPA and Si surface measured experimentally,⁶⁴ the theoretical range from -1.1 to -1.3 eV for the TiO_2 -dopamine bond strength,⁶⁵ and -1.5 eV for the

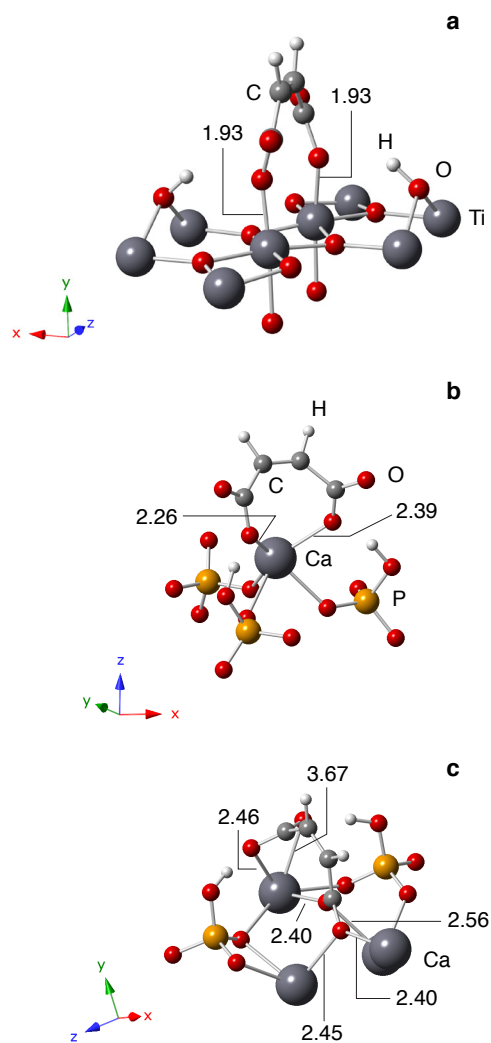


Figure 6: Maleic acid and neighbour atoms of the adsorption complex (a) at the (110) surface of TiO_2 , (b) at the HA (0001) surface, and (c) at the HA (01 $\bar{1}$ 0) surface. Bond distances between the maleic acid and surface metal atoms are shown in Angstroms for an aqueous environment.

caffeic acid adsorption on TiO_2 in vacuum.

Effect of the solution pH on adsorption energies can be accounted by evaluating a change in the free energy of a residue as a result of deprotonation⁶⁶

$$\Delta G = -RT \ln 10(\text{pH} - \text{p}K_{\text{a}}), \tag{3}$$

where R is the gas constant, T is the temperature, and $\text{p}K_{\text{a}}$ is a dissociation constant. The dissociation constants for MA are $\text{p}K_{\text{a}1} = 1.9$ and $\text{p}K_{\text{a}2} = 6.0$.⁶⁷ This implies that both carboxyl groups are deprotonated at the experimental conditions ($\text{pH} = 7$). As a result, the free energy of MA is lowered by $\Delta G \approx -0.16$ eV per residue (-0.10 and -0.06 eV for the first and second group, respectively). To account for deprotonation, the magnitude of adsorption enthalpies in Table 2 should be corrected by the corresponding value of ΔG , which results in reduction of the magnitude of the adsorption energy with increasing pH value but does not prevent MA residues from adsorption as observed experimentally by Hidber et al.⁴.

Next we continue with an experimental verification of theoretical predictions. It should be emphasized once again that individual MA monomers are used in the modeling section for the sake of computational simplicity, while PSMA-h copolymers are employed in the experimental section to provide multiple chemical bonds with substrates. Due to the limitations of the concept of zeta-potential for analysis of particles, containing adsorbed polyelectrolytes,⁶⁸⁻⁷⁰ the influence of PSMA-h adsorption on the electrokinetic behavior of the TiO_2 (rutile) particles was analyzed using the EPD yield data. The EPD experiments performed with the $5-10 \text{ g L}^{-1}$ TiO_2 (rutile) suspensions without PSMA-h showed the formation of cathodic deposits. The low cathodic EPD yield indicated that particles were weakly positively charged. PSMA-h films were deposited anodically and showed strong adhesion to the substrates. The film adhesion corresponded to 5B classification (ASTM D3359). The addition of PSMA-h to the TiO_2 suspensions resulted in significant improvement of the suspension stability and formation of anodic deposits. The formation of anodic films signified a particle charge re-

versal due to the adsorption of the negatively charged PSMA-h. The deposit mass increased with increasing deposition time at a constant applied voltage (Fig. 7). The experimental results indicated that the film thickness can be controlled and varied. The deposition yield data showed relatively high deposition rate. A decrease of deposition rate with time was observed due to the reduction in the voltage drop in the bulk of the suspension as a result of the formation of an insulating film layer on the electrode surface.

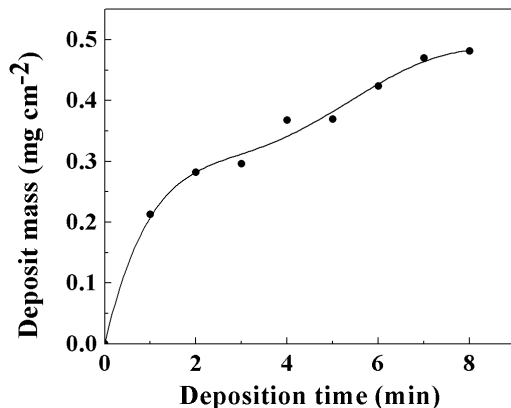


Figure 7: Deposit mass versus deposition time for 5 g L^{-1} TiO_2 suspension, containing 10 g L^{-1} PSMA-h at a deposition voltage of 15 V.

The PSMA-h adsorption on the TiO_2 particles was confirmed by the FTIR analysis (Fig. 8) of the deposited material. Figure 8 shows absorption peaks at 1453 , 1493 cm^{-1} related to C–C vibrations of the aromatic rings of the styrene monomers and another absorption at 1709 cm^{-1} attributed to C=O vibrations of the MA monomers of the adsorbed polymer.

SEM studies showed the formation of continuous and crack-free TiO_2 -PSMA-h films (Fig. 9). It was found that the variation of TiO_2 concentration in the suspension resulted in changes of film microstructure. The SEM image of a film, prepared from the 5 g L^{-1} TiO_2 suspension, containing 10 g L^{-1} PSMA-h showed TiO_2 particles in a PSMA-h matrix (Fig. 9a). The SEM image of the film prepared from 10 g L^{-1} TiO_2 suspension (Fig. 9b), containing 10 g L^{-1} PSMA-h showed mainly TiO_2 particles, which formed a porous film. The film porosity resulted from packing of TiO_2 particles. The comparison of the SEM

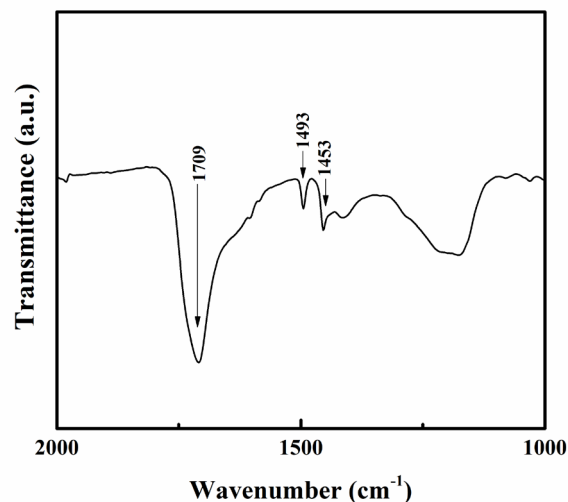


Figure 8: FTIR spectrum of a deposit, obtained from a suspension, containing 10 g L^{-1} TiO_2 and 10 g L^{-1} PSMA-h.

images, shown in Fig. 9a,b, indicated that the increase of TiO_2 concentration in the 10 g L^{-1} PSMA-h solution resulted in the increasing TiO_2 content in the deposited film.

The composite TiO_2 -PSMA-h coating prepared from 5 g L^{-1} TiO_2 suspension, containing 10 g L^{-1} PSMA-h, was studied in Hank's balanced salt solution, which acted as a simulated body fluid. Tafel plots comparing the electrochemical behaviour of the coated and uncoated titanium are shown in Fig. 10. From the Tafel plots it can be seen that deposited TiO_2 -PSMA-h coating allowed a reduction of the corrosion current, compared to an uncoated titanium. Moreover, the coated substrate showed a higher corrosion potential. These results demonstrated that the coating acted as a protective layer and provided corrosion protection of the titanium substrates. Therefore the TiO_2 -PSMA-h coating, containing the bioactive TiO_2 rutile phase offers additional benefits of corrosion protection of underlying metallic substrates for biomedical implant applications.

Related to biomedical applications, we investigated PSMA-h as a co-dispersant for the co-deposition of TiO_2 (rutile) and HA to fabricate composite rutile-HA coatings. A suspension containing 5 g L^{-1} HA, 5 g L^{-1} TiO_2 and 10 g L^{-1} PSMA-h was used for anodic EPD, and subsequent films were studied using XRD. The resulting X-ray diffraction pattern is shown

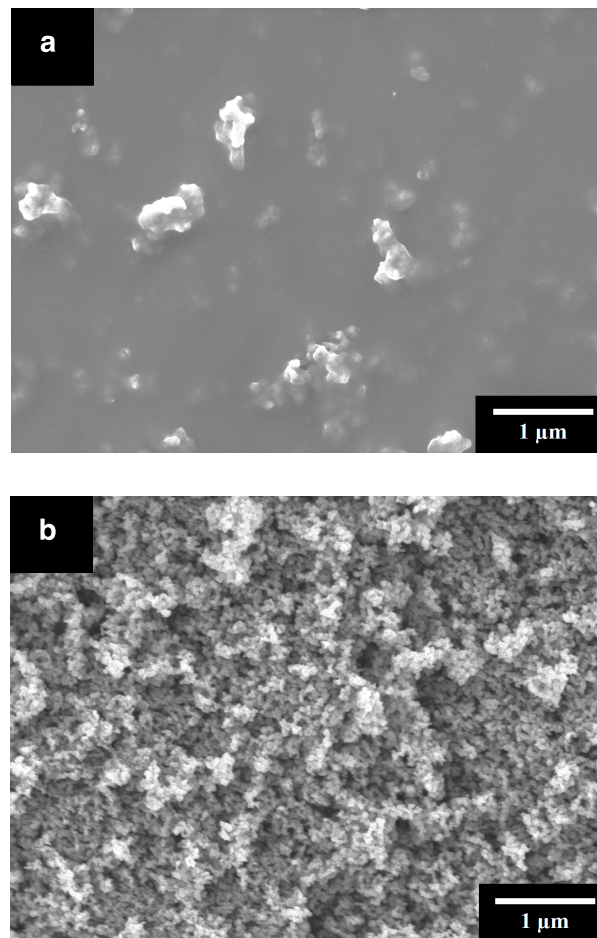


Figure 9: SEM images of deposits, prepared from (a) 5 and (b) 10 g L⁻¹ TiO₂ suspension, containing 10 g L⁻¹ PSMA-h at a deposition voltage of 10 V.

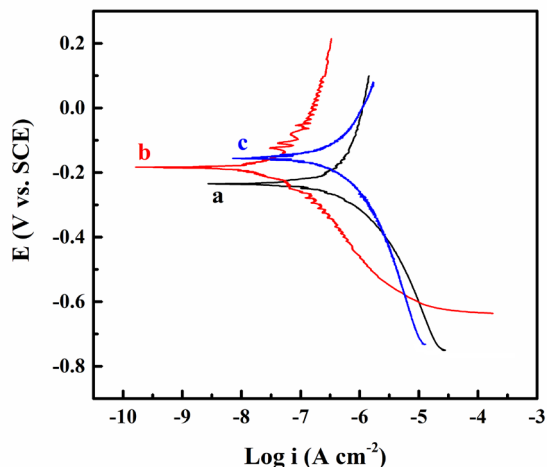


Figure 10: Tafel plots in Hank's solutions for (a) uncoated Ti, (b) coated by deposition from 5 g L^{-1} TiO_2 suspension, containing 10 g L^{-1} PSMA-h and (c) coated by deposition from a suspension, containing 5 g L^{-1} TiO_2 , 5 g L^{-1} HA and 10 g L^{-1} PSMA-h at a deposition voltage of 10 V during 5 min.

in Fig. 11. The XRD pattern showed TiO_2 (rutile) peaks, corresponding to the JCPDS file 021-1276 and peaks of HA, corresponding to the JCPDS file 046-0905. This confirmed that HA and TiO_2 were co-deposited using PSMA-h, and thus composite HA-rutile-PSMA-h films were formed. The results of SEM studies (Fig. 12) provided additional evidence of the formation of composite coatings. The SEM image presented in Fig. 12 shows needle-shape HA particles in addition to the TiO_2 particles. Therefore, PSMA-h can be used as a co-dispersing and film-forming agent for the co-deposition of HA and rutile. The composite coatings showed corrosion protection of Ti substrates, as indicated (Fig. 10) by the increase in the corrosion potential and reduction of the corrosion current. As emphasised above, the composite coating containing HA and rutile offer many benefits for biomedical application. EPD method has many processing advantages, such as high deposition rate and possibility of uniform deposition on substrates of complex shape and high surface area.

Finally, we would like to comment on an interference between adsorption of MA and hydration of surface by chemisorption of water molecules that takes place under relevant experimental conditions. The hydration of metal oxides is governed by the following two-

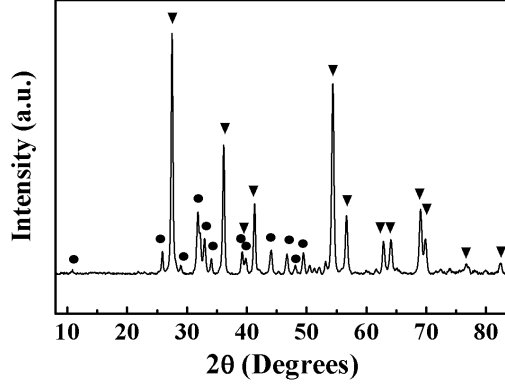


Figure 11: X-ray diffraction pattern of a composite coating, prepared from a suspension, containing 5 g L^{-1} HA and 5 g L^{-1} TiO_2 , containing 10 g L^{-1} PSMA-h at a deposition voltage of 10 V (▼- TiO_2 rutile, ●-HA).

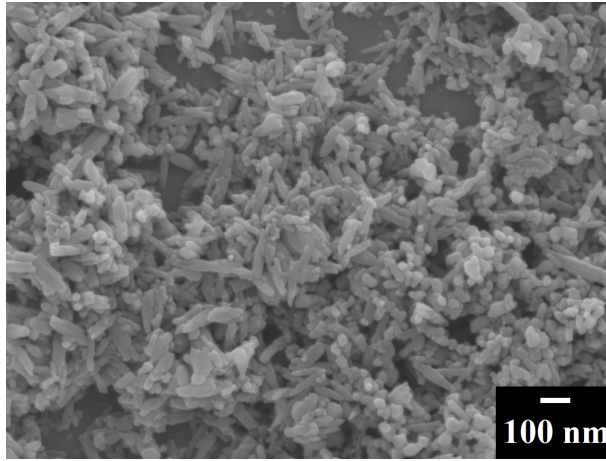
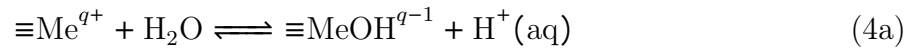


Figure 12: SEM image of the composite film, prepared from the suspensions, containing 5 g L^{-1} TiO_2 , 5 g L^{-1} HA and 10 g L^{-1} PSMA-h.

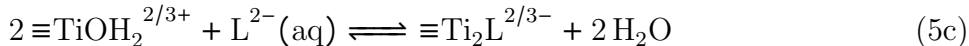
step reaction



Here $\equiv\text{Me}$ is a surface metal ion (either Ti or Ca), and q indicates its fractional charge. The charge is $q = 2/3e$ for rutile (110) surface,⁶² where e is the elementary charge. The HA(01 $\bar{1}$ 0) surface has several $\equiv\text{Ca}^{q+}$ and $\equiv\text{O}^{q-}$ sites with a range of q -values up to $1e$ due to a variety of dangling bonds created in the process of cleaving the surface (see Fig. 2).

Results for the enthalpy of water molecule chemisorption at these two surfaces are listed in Table 3. The water chemisorption is favourable at both surfaces in vacuum, which agrees with previous studies.^{57,71} However, the presence of solvent not only reduces the magnitude of interaction but also changes the surface receptivity. As evident from Table 3, the enthalpy of dissociative adsorption of water molecules at the HA(011 $\bar{1}$ 0) surface in aqueous environment is positive, indicating that its chemisorption is unlikely. When reflected onto experimental conditions, this result implies that the surface of rutile particles is likely to be terminated with hydroxyl groups during a reaction with PSMA-h, whereas the surface of HA is not. As a benchmark for the solvation model we also computed the vaporization enthalpy of water molecule +0.32 eV *vs* the experimental value of +0.46 eV,⁷² which sets error-bars of the calculation.

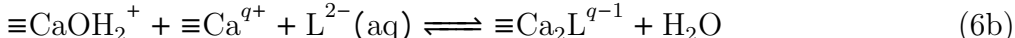
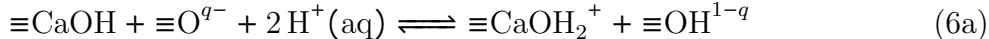
Adsorption of MA on the rutile (110) surface in the presence of surface hydroxyl groups is described as a multistep ligand (L) exchange reaction^{4,73}



which involves deprotonation of the ligand, protonation of surface hydroxyl groups on Ti-site, and finally the ligand exchange. This reaction leads to desorption of two water molecules from the surface of TiO₂, which is energetically unlikely in an aqueous environment due to reasons discussed in the preceding paragraph. As a result, an enthalpy is positive for the ligand exchange reaction between hydroxyl groups at the TiO₂ surface and MA monomer or MA segment as a part of PSMA-h (Table 3). To explain the experimentally observed adsorption of PSMA-h on TiO₂, we recall that the adsorption takes place in a water-ethanol solution. In their experimental study of adsorption of alcohols on TiO₂ (rutile) surface, Suda et al.⁷⁴ noted that ethanol adsorption to the surface results in expelling water

from the surface, which implies presence of $\equiv\text{Ti}^{2/3+}$ bonding site at the surface with no need for the ligand exchange.

The absence of a strong dissociative bond between water and HA allows us to assume coexistence of the hydrated $\equiv\text{CaOH}$ and $\equiv\text{OH}$ surface sites with unhydrated $\equiv\text{Ca}^{q+}$ and $\equiv\text{O}^{q-}$ sites. The ligand exchange reaction in this case proceeds through the following steps



The corresponding enthalpy is strongly negative (see Table 3) indicating that, unlike in the case of TiO_2 , there is no competition between water chemisorption and MA adsorption at the surface of HA.

Table 3: Chemisorption enthalpy of water and MA molecules at rutile (110) and HA(01 $\bar{1}$ 0) surfaces calculated in a gas phase and in an aqueous solution.

Species	Reactions	Enthalpy (eV)	
		in gas phase	aq. solution
H_2O on TiO_2	Eq. (4)	-0.9	-0.4
H_2O on HA	Eq. (4)	-1.8	+0.3
MA monomer on TiO_2	Eq. (5)	—	+0.3
MA segment on TiO_2	Eq. (5)	—	+0.4
MA monomer on HA	Eqs.(5a) and (6)	—	-2.2
MA segment on HA	Eqs.(5a) and (6)	—	-1.6

4 Conclusions

Poly(styrene-alt-maleic acid) adsorption on hydroxyapatite and TiO_2 (rutile) was studied using experimental techniques and corroborated by *ab initio* simulations of adsorption of a maleic acid segment as a subunit of the copolymer. *Ab initio* calculations suggest that the maleic acid segment adsorbs to the TiO_2 surface *via* an inner sphere bridge bidentate bonding to a pair of Ti-atoms. Chelation is a preferable type of bonding for the maleic acid

segment on hydroxyapatite due to peculiarities of the surface reconstruction. The aliphatic nature of maleic acid makes it adaptive to various surfaces with a little energy penalty (of the order 0.15 eV) associated with structural changes such as flattening. A magnitude of the adsorption enthalpy for the maleic acid monomer and the segment is comparable to that of catecholates. Solvent effects play a twofold role when providing quantitative evaluation of the adsorption energies and, thus, cannot be neglected. First, it significantly reduces the adsorption strength (by almost factor of two if compared to vacuum) as the polarity of the solvent increases. Second, a water chemisorption at the surface hinders the adsorption of maleic acid at the surface of rutile. The results of first-principle calculations were confirmed by the experimental measurements. We found that adsorbed poly(styrene-alt-maleic acid) allowed efficient dispersion of rutile and formation of films by the electrophoretic deposition. We investigated the deposition yield and morphology of the films. Moreover, it was found that rutile can be co-dispersed and co-deposited with hydroxyapatite to form composite films. The coatings obtained by the electrophoretic deposition showed corrosion protection of metallic implants in simulated body fluid solutions, which is a favorable characteristic for biomedical applications.

Acknowledgement

M.A. and O.R. would like to acknowledge the funding provided by the Natural Sciences and Engineering Research Council of Canada under the Discovery Grant Program RGPIN-2015-04518. The computations were performed using Compute Canada (Calcul Quebec and Compute Ontario) resources, including the infrastructure funded by the Canada Foundation for Innovation. A.C. and I.Zh. would like to acknowledge the funding provided by the Natural Sciences and Engineering Research Council of Canada under the Strategic Project 447475-13.

Notes

There are no conflicts to declare.

References

- (1) Xu, A.-W.; Ma, Y.; Cölfen, H. Biomimetic mineralization. *J. Mater. Chem.* **2007**, *17*, 415–449.
- (2) Lee, H.; Dellatore, S. M.; Miller, W. M.; Messersmith, P. B. Mussel-Inspired Surface Chemistry for Multifunctional Coatings. *Science* **2007**, *318*, 426–430.
- (3) Lee, B. P.; Messersmith, P.; Israelachvili, J.; Waite, J. Mussel-Inspired Adhesives and Coatings. *Annu. Rev. Mater. Res.* **2011**, *41*, 99–132.
- (4) Hidber, P. C.; Graule, T. J.; Gauckler, L. J. Influence of the dispersant structure on properties of electrostatically stabilized aqueous alumina suspensions. *J. Eur. Ceram. Soc.* **1997**, *17*, 239–249.
- (5) Lee, H.; Lee, B. P.; Messersmith, P. B. A reversible wet/dry adhesive inspired by mussels and geckos. *Nature* **2007**, *448*, 338–341.
- (6) Ata, M. S.; Liu, Y.; Zhitomirsky, I. A review of new methods of surface chemical modification, dispersion and electrophoretic deposition of metal oxide particles. *RSC Adv.* **2014**, *4*, 22716–22732.
- (7) Clifford, A.; Ata, M. S.; Zhitomirsky, I. Synthesis, liquid – liquid extraction and deposition of hydroxyapatite nanorod composites. *Mater. Lett.* **2017**, *201*, 140–143.
- (8) Chen, R.; Ata, M. S.; Zhao, X.; Clifford, A.; Puri, I.; Zhitomirsky, I. Strategies for liquid-liquid extraction of oxide particles for applications in supercapacitor electrodes and thin films. *J. Colloid Interface Sci.* **2017**, *499*, 1–8.

- (9) Poon, R.; Zhao, X.; Ata, M. S.; Clifford, A.; Zhitomirsky, I. Phase transfer of oxide particles for application in thin films and supercapacitors. *Ceram. Int.* **2017**, *43*, 8314–8320.
- (10) Wallar, C.; Zhang, T.; Shi, K.; Zhitomirsky, I. Synthesis of metal and metal oxide nanoparticles, liquid-liquid extraction and application in supercapacitors. *Colloids Surf. A* **2016**, *500*, 195–202.
- (11) Ye, Q.; Zhou, F.; Liu, W. Bioinspired catecholic chemistry for surface modification. *Chem. Soc. Rev.* **2011**, *40*, 4244–4258.
- (12) Dobson, K. D.; McQuillan, A. In situ infrared spectroscopic analysis of the adsorption of aliphatic carboxylic acids to TiO₂, ZrO₂, Al₂O₃, and Ta₂O₅ from aqueous solutions. *Spectrochim. Acta Mol. Biomol. Spectrosc.* **1999**, *55*, 1395–1405.
- (13) Lenhart, J. J.; Heyler, R.; Walton, E. M.; Mylon, S. E. The influence of dicarboxylic acid structure on the stability of colloidal hematite. *J. Colloid Interface Sci.* **2010**, *345*, 556–560.
- (14) Pujari, S. P.; Scheres, L.; Marcelis, A. T. M.; Zuilhof, H. Covalent Surface Modification of Oxide Surfaces. *Angew. Chem. Int. Ed.* **2014**, *53*, 6322–6356.
- (15) Gaponik, N.; Talapin, D. V.; Rogach, A. L.; Eychmüller, A.; Weller, H. Efficient Phase Transfer of Luminescent Thiol-Capped Nanocrystals: From Water to Nonpolar Organic Solvents. *Nano Lett.* **2002**, *2*, 803–806.
- (16) Gao, X.; Tam, K.; Yu, K. M. K.; Tsang, S. C. Synthesis and Characterization of Thiol-Capped FePt Nanomagnetic Porous Particles. *Small* **2005**, *1*, 949–952.
- (17) Paul, A.; Kaverina, E.; Vasiliev, A. Synthesis of silver/polymer nanocomposites by surface coating using carbodiimide method. *Colloids Surf. A* **2015**, *482*, 44–49.

- (18) Mohanty, S.; Das, B.; Dhara, S. Poly(maleic acid) – A novel dispersant for aqueous alumina slurry. *J. Am. Ceram. Soc.* **2013**, *1*, 184–190.
- (19) Blockhaus, F.; Sequaris, J.-M.; Narres, H.; Schwuger, M. Adsorption–desorption behavior of acrylic–maleic acid copolymer at clay minerals. *J. Colloid Interface Sci.* **1997**, *186*, 234–247.
- (20) Zhao, J.; Wang, X.; Gui, Z.; Li, L. Dispersion of barium titanate with poly(acrylic acid-co-maleic acid) in aqueous media. *Ceram. Int.* **2004**, *30*, 1985–1988.
- (21) Lai, C.-T.; Hong, J.-L. Role of Concentration on the Formulation of Zinc Oxide Nanorods from Poly(styrene- alt -maleic acid) Template. *J. Phys. Chem. C* **2009**, *113*, 18578–18583.
- (22) Yu, J.; Tang, H.; Cheng, B.; Zhao, X. Morphological control of calcium oxalate particles in the presence of poly-(styrene-alt-maleic acid). *J. Solid State Chem.* **2004**, *177*, 3368–3374.
- (23) Yu, J.; Guo, H.; Cheng, B. Shape evolution of SrCO₃ particles in the presence of poly-(styrene-alt-maleic acid). *J. Solid State Chem.* **2006**, *179*, 800–803.
- (24) Xu, A.-W.; Antonietti, M.; Yu, S.-H.; Cölfen, H. Polymer-Mediated Mineralization and Self-Similar Mesoscale-Organized Calcium Carbonate with Unusual Superstructures. *Adv. Mater.* **2008**, *20*, 1333–1338.
- (25) Henry, S. M.; El-Sayed, M. E. H.; Pirie, C. M.; Hoffman, A. S.; Stayton, P. S. pH-responsive poly(styrene-alt-maleic anhydride) alkylamide copolymers for intracellular drug delivery. *Biomacromolecules* **2006**, *7*, 2407–2414.
- (26) Dalela, M.; Shrivastav, T. G.; Kharbanda, S.; Singh, H. pH-sensitive biocompatible nanoparticles of paclitaxel-conjugated poly(styrene- co -maleic acid) for anticancer drug

- delivery in solid tumors of syngeneic mice. *ACS Appl. Mater. Interfaces* **2015**, *7*, 26530–26548.
- (27) Angelova, N.; Yordanov, G. Nanoparticles of poly(styrene-co-maleic acid) as colloidal carriers for the anticancer drug epirubicin. *Colloids Surf. A* **2014**, *452*, 73–81.
- (28) Baghayeri, M.; Zare, E. N.; Namadchian, M. Direct electrochemistry and electrocatalysis of hemoglobin immobilized on biocompatible poly(styrene-alternative-maleic acid)/functionalized multi-wall carbon nanotubes blends. *Sens. Actuator B-Chem.* **2013**, *188*, 227–234.
- (29) Samoilova, N.; Kurskaya, E.; Krayukhina, M.; Askadsky, A.; Yamskov, I. Copolymers of maleic acid and their amphiphilic derivatives as stabilizers of silver nanoparticles. *J. Phys. Chem. B* **2009**, *113*, 3395–3403.
- (30) Saez-Martinez, V.; Punyamoonwongsa, P.; Tighe, B. J. Polymer–lipid interactions: Biomimetic self-assembly behaviour and surface properties of poly(styrene-alt-maleic acid) with diacylphosphatidylcholines. *React. Funct. Polym.* **2015**, *94*, 9–16.
- (31) Hongkachern, T.; Champreda, V.; Sriksirin, T.; Wangkam, T.; Osotchan, T. Effect of pH on the formation of a bovine serum albumin layer on a poly(styrene-co-maleic acid) surface. *Adv. Mat. Res.* **2010**, *93–94*, 583–586.
- (32) Clifford, A.; Luo, D.; Zhitomirsky, I. Colloidal strategies for electrophoretic deposition of organic-inorganic composites for biomedical applications. *Colloids Surf. A* **2017**, *516*, 219–225.
- (33) Boccaccini, A. R.; Keim, S.; Ma, R.; Li, Y.; Zhitomirsky, I. Electrophoretic deposition of biomaterials. *J. R. Soc. Interface* **2010**, *7*, S581–S613.
- (34) Cai, Y.; Li, H.; Karlsson, M.; Leifer, K.; Engqvist, H.; Xia, W. Biom mineralization on

- single crystalline rutile: the modulated growth of hydroxyapatite by fibronectin in a simulated body fluid. *RSC Adv.* **2016**, *6*, 35507–35516.
- (35) Lindahl, C.; Borchardt, P.; Lausmaa, J.; Xia, W.; Engqvist, H. Studies of early growth mechanisms of hydroxyapatite on single crystalline rutile: A model system for bioactive surfaces. *J. Mater. Sci.: Mater. Med.* **2010**, *21*, 2743–2749.
- (36) Lu, X.; Zhang, H.-p. P.; Leng, Y.; Fang, L.; Qu, S.; Feng, B.; Weng, J.; Huang, N. The effects of hydroxyl groups on Ca adsorption on rutile surfaces: A first-principles study. *J. Mater. Sci.: Mater. Med.* **2010**, *21*, 1–10.
- (37) Kasemanankul, P.; Witit-Anan, N.; Chaiyakun, S.; Limsuwan, P.; Boonamnuayvitaya, V. Low-temperature deposition of (110) and (101) rutile TiO₂ thin films using dual cathode DC unbalanced magnetron sputtering for inducing hydroxyapatite. *Mater. Chem. Phys.* **2009**, *117*, 288–293.
- (38) Xiao, X. F.; Liu, R. F.; Zheng, Y. Z. Characterization of hydroxyapatite/titania composite coatings codeposited by a hydrothermal-electrochemical method on titanium. *Surf. Coat. Technol.* **2006**, *200*, 4406–4413.
- (39) Ulasevich, S. A.; Kulak, A. I.; Poznyak, S. K.; Karpushenkov, S. A.; Lisenkov, A. D.; Skorb, E. V. Deposition of hydroxyapatite- \check{u} incorporated TiO₂ coating on titanium using plasma electrolytic oxidation coupled with electrophoretic deposition. *RSC Adv.* **2016**, *6*, 62540–62544.
- (40) Jaworski, R.; Pawlowski, L.; Pierlot, C.; Roudet, F.; Kozerski, S.; Petit, F. Recent developments in suspension plasma sprayed titanium oxide and hydroxyapatite coatings. *J. Therm. Spray Technol.* **2010**, *19*, 240–247.
- (41) Hannora, A. E.; Ataya, S. Structure and compression strength of hydroxyapatite/titania nanocomposites formed by high energy ball milling. *J. Alloys Compd.* **2016**, *658*, 222–233.

- (42) Sarao, T. P. S.; Sidhu, H. S.; Singh, H. Characterization and In Vitro Corrosion Investigations of Thermal Sprayed Hydroxyapatite and Hydroxyapatite-Titania Coatings on Ti Alloy. *Metall. Mater. Trans. A* **2012**, *43*, 4365–4376.
- (43) Kohn, W.; Sham, L. J. Self-Consistent Equations Including Exchange and Correlation Effects. *Phys. Rev.* **1965**, *140*, A1133–A1138.
- (44) Perdew, J. P.; Burke, K.; Ernzerhof, M. Generalized Gradient Approximation Made Simple. *Phys. Rev. Lett.* **1996**, *77*, 3865–3868.
- (45) Blöchl, P. E. Projector augmented-wave method. *Phys. Rev. B* **1994**, *50*, 17953–17979.
- (46) Kresse, G.; Joubert, D. From ultrasoft pseudopotentials to the projector augmented-wave method. *Phys. Rev. B* **1999**, *59*, 1758–1775.
- (47) Kresse, G.; Furthmüller, J. Efficient iterative schemes for ab initio total-energy calculations using a plane-wave basis set. *Phys. Rev. B* **1996**, *54*, 11169–11186.
- (48) Monkhorst, H. J.; Pack, J. D. Special points for Brillouin-zone integrations. *Phys. Rev. B* **1976**, *13*, 5188–5192.
- (49) Dudarev, S. L.; Botton, G. A.; Savrasov, S. Y.; Humphreys, C. J.; Sutton, A. P. Electron-energy-loss spectra and the structural stability of nickel oxide: An LSDA+U study. *Phys. Rev. B* **1998**, *57*, 1505–1509.
- (50) Hu, Z.; Metiu, H. Choice of U for DFT+U calculations for titanium oxides. *J. Phys. Chem. C* **2011**, *115*, 5841–5845.
- (51) Howard, C. J.; Sabine, T. M.; Dickson, F. Structural and thermal parameters for rutile and anatase. *Acta Cryst. B* **1991**, *47*, 462–468.
- (52) Kay, M. I.; Young, R. A.; Posner, A. S. Crystal structure of hydroxyapatite. *Nature* **1964**, *204*, 1050–1052.

- (53) Ramamoorthy, M.; Vanderbilt, D.; King-Smith, R. D. First-principles calculations of the energetics of stoichiometric TiO₂ surfaces. *Phys. Rev. B* **1994**, *49*, 16721–16727.
- (54) Bullard, J. W.; Cima, M. J. Orientation dependence of the isoelectric point of TiO₂ (rutile) surfaces. *Langmuir* **2006**, *22*, 10264–10271.
- (55) Zhu, W.; Wu, P. Surface energetics of hydroxyapatite: A DFT study. *Chem. Phys. Lett.* **2004**, *396*, 38–42.
- (56) Almora-Barrios, N.; de Leeuw, N. H. A Density Functional Theory Study of the Interaction of Collagen Peptides with Hydroxyapatite Surfaces. *Langmuir* **2010**, *26*, 14535–14542.
- (57) Chiatti, F.; Delle Piane, M.; Ugliengo, P.; Corno, M. Water at hydroxyapatite surfaces: the effect of coverage and surface termination as investigated by all-electron B3LYP-D* simulations. *Theor. Chem. Acc.* **2016**, *135*, 54.
- (58) Mathew, K.; Sundararaman, R.; Letchworth-Weaver, K.; Arias, T. A.; Hennig, R. G. Implicit solvation model for density-functional study of nanocrystal surfaces and reaction pathways. *J. Chem. Phys.* **2014**, *140*, 084106.
- (59) Wohlfarth, C. In *Supplement to IV/6. Landolt-Börnstein – Group IV Physical Chemistry (Numerical Data and Functional Relationships in Science and Technology)*; Lechner, M. D., Ed.; Springer, Berlin, Heidelberg, 2008; Chapter Dielectric constant of the mixture (1) water; (2) ethanol, pp 520–523.
- (60) Bourikas, K.; Kordulis, C.; Lycourghiotis, A. Titanium Dioxide (Anatase and Rutile): Surface Chemistry, Liquid–Solid Interface Chemistry, and Scientific Synthesis of Supported Catalysts. *Chem. Rev.* **2014**, *114*, 9754–9823.
- (61) Zhao, W.; Xu, Z.; Yang, Y.; Sahai, N. Surface energetics of the hydroxyapatite

- nanocrystal-water interface: a molecular dynamics study. *Langmuir* **2014**, *30*, 13283–13292.
- (62) Zhang, T.; Wojtal, P.; Rubel, O.; Zhitomirsky, I. Density functional theory and experimental studies of caffeic acid adsorption on zinc oxide and titanium dioxide nanoparticles. *RSC Adv.* **2015**, *5*, 106877–106885.
- (63) Gross, A.; Scheffler, M. Role of zero-point effects in catalytic reactions involving hydrogen. *J. Vac. Sci. Technol. A* **1997**, *15*, 1624–1629.
- (64) Lee, H.; Scherer, N. F.; Messersmith, P. B. Single-molecule mechanics of mussel adhesion. *Proc. Natl. Acad. Sci. U.S.A.* **2006**, *103*, 12999–13003.
- (65) Vega-Arroyo, M.; LeBreton, P. R.; Rajh, T.; Zapol, P.; Curtiss, L. A. Density functional study of the TiO₂-dopamine complex. *Chem. Phys. Lett.* **2005**, *406*, 306–311.
- (66) Bombarda, E.; Ullmann, G. M. pH-Dependent pK_a Values in Proteins—A Theoretical Analysis of Protonation Energies with Practical Consequences for Enzymatic Reactions. *J. Phys. Chem. B* **2010**, *114*, 1994–2003.
- (67) Pirrone, V.; Passic, S.; Wigdahl, B.; Rando, R. F.; Labib, M.; Krebs, F. C. A Styrene-alt -Maleic Acid Copolymer Is an Effective Inhibitor of R5 and X4 Human Immunodeficiency Virus Type 1 Infection. *J. Biomed. Biotechnol.* **2010**, *2010*, 548749.
- (68) Zhitomirsky, I. Cathodic electrodeposition of ceramic and organoceramic materials. Fundamental aspects. *Adv. Colloid Interface Sci.* **2002**, *97*, 279–317.
- (69) Ohshima, H. Electrophoretic mobility of soft particles. *Colloids Surf. A* **1995**, *103*, 249–255.
- (70) Ohshima, H. Dynamic electrophoretic mobility of a soft particle. *J. Colloid Interface Sci.* **2001**, *233*, 142–152.

- (71) Zheng, T.; Wu, C.; Chen, M.; Zhang, Y.; Cummings, P. T. A DFT study of water adsorption on rutile TiO₂ (110) surface: The effects of surface steps. *J. Chem. Phys.* **2016**, *145*, 044702.
- (72) Cox, J. D.; Wagman, D. D.; Medvedev, V. A. *CODATA key values for thermodynamics*; Hemisphere Publishing Corp.: New York, 1989.
- (73) Rodriguez, R.; Blesa, M. A.; Regazzoni, A. E. Surface Complexation at the TiO₂(anatase)/Aqueous Solution Interface: Chemisorption of Catechol. *J. Colloid Interface Sci.* **1996**, *177*, 122–131.
- (74) Suda, Y.; Morimoto, T.; Nagao, M. Adsorption of alcohols on titanium dioxide (rutile) surface. *Langmuir* **1987**, *3*, 99–104.

Graphical TOC Entry

